

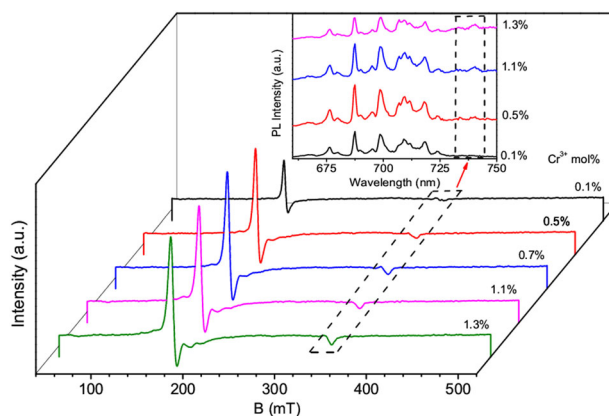
Influence of inversion defects and Cr–Cr pairs on the photoluminescent performance of ZnAl_2O_4 crystals

Dong Zhang^{1,2} · Qingjie Guo¹ · Yanfang Ren¹ · Changzheng Wang³ · Qiang Shi^{1,2} · Qinglin Wang^{1,2} · Xia Xiao^{1,2} · Wenjun Wang^{1,2} · Quli Fan^{1,4}

Received: 19 July 2017 / Accepted: 11 October 2017 / Published online: 25 October 2017
© Springer Science+Business Media, LLC 2017

Abstract $\text{ZnAl}_2\text{O}_4:\text{Cr}^{3+}$ crystals were synthesized by using sol–gel method at 1000 °C. The results showed that with the concentration of Cr^{3+} in spinel lattices increasing, the x-ray diffraction peaks shifted toward lower diffraction angles, and the grain size revealed a rapid increase and became invariable when the Cr^{3+} dopant concentration was above 0.7 mol%. All the samples showed a series of emission peaks ranging from 660 to 730 nm assigned to spin-forbidden ${}^2\text{E}_g \rightarrow {}^4\text{A}_{2g}$ transition of Cr^{3+} ions in spinel lattices. The intensity of emission peaks revealed a strong dependence on the Cr^{3+} concentration. An additional emission peak at 740 nm was present when the Cr^{3+} ions concentration was above 0.5%. All emission peaks were quenched when the Cr^{3+} concentration reaches 1.3 mol%. The results of x-ray photoelectron spectroscopy (XPS) and electron paramagnetic resonance (EPR) suggested that the Cr^{3+} ions occupied the octahedral sites in spinel lattices, and with the Cr^{3+} concentration increasing, the exchange interaction and coupling interaction between Cr–Cr were enhanced and the antisite defects related to Zn in octahedral sites increased.

Graphical abstract



Keywords Semiconductors · Zinc Aluminate · Microstructures · Photoluminescence

1 Introduction

Zinc aluminate (ZnAl_2O_4) has attracted considerable attention due to its desirable properties, such as high mechanical resistance, high thermal stability, low surface acidity, and hydrophobicity. These characteristics make it very suitable for applications in the field of high-temperature material, catalyst, catalyst support, ceramic pigment, and optical and thermal control coating for spacecraft [1–6]. As one of the best wide-band-gap semiconductor ($E_g = 3.8\text{ eV}$), ZnAl_2O_4 is emerging as an important material in UV optoelectronic devices. ZnAl_2O_4 is a normal spinel structure with Zn^{2+} occupying tetrahedral sites and Al^{3+} occupying octahedral sites of the structure.

✉ Dong Zhang
physzd@foxmail.com

¹ School of Physical Science and Information Technology, Liaocheng University, 252059 Liaocheng, China
² Shandong Provincial Key Laboratory of Optical Communication Science and Technology, 252059 Shandong, China
³ School of Materials Engineering, Liaocheng University, 252059 Liaocheng, China
⁴ Institute of Advanced Materials, Nanjing University of Posts and Telecommunications, 210023 Nanjing, China

Some defects related to vacancies and antisites are present in the spinel type of crystals synthesized at various conditions [7, 8]. Sreeja et al. [9] investigated the size dependence of coordination behavior and cation distribution in MgAl_2O_4 nanoparticles from ^{27}Al solid state by using nuclear magnetic resonance (NMR) studies. They have showed that the oxygen vacancies and antisite defects were related to Al replacing Mg (Al_{Mg}), which were presented in the crystal surface, and showed that the percentage of Al ions in the tetrahedral sites decreased with increasing particle size. Besides, their indirect evidence indicated that the inversion defects related to Mg occupying Al sites existed in spinel structure. The theoretical results suggested that the formation energy of antisite defects between Zn and Al ions was lower than that of metal vacancies [8] and the antisite defects coexisted in zinc aluminate crystals [10].

As a kind of excellent optical host materials, zinc aluminate crystals were doped with various rare earth (RE) elements, such as Eu^{3+} , Dy^{3+} , Tb^{3+} , Ce^{3+} , and so on, to obtain the higher efficient luminescent with different wavelengths [11–14]. Due to the high cost of RE, the transition elements as a substitute for RE elements have attracted more attention recently. Different from the RE elements occupying the octahedral (Al^{3+}) sites, the transition elements usually occupy the octahedral and tetrahedral sites due to their rich valences. The green emission is observed in $\text{ZnAl}_2\text{O}_4:\text{Mn}^{2+}$ crystals, in which the Mn^{2+} ions occupied Zn^{2+} sites, while the red emission was excited when the Mn^{3+} and Mn^{4+} ions occupied the Al^{3+} sites [15–17]. The violet, blue, and green emissions were observed in ZnAl_2O_4 particles doped with Co^{2+} ions [18]. The higher efficient blue emissions from $\text{ZnAl}_2\text{O}_4:\text{Ti}$ nanocrystals were reported by Tsai et al. [19], which was related to the charge-transfer transitions between $\text{O}^{2-}-\text{Ti}^{4+}$ and $\text{O}^{2-}-\text{Ti}^{3+}$ ion pairs. The results from Dereń et al. [20] suggested that the emission color depended on the nanocrystal size and changed from violet to blue with an increase of the diameter due to the additional levels created by oxygen, zinc, and aluminum vacancies in the gahnite. Because of the wide photoluminescence (PL) emission peak, it is hard to observe the influence of inversion defects in gahnite on the emission peaks. As excellent emission centers, Cr^{3+} ions are doped in Al_2O_3 crystals to obtain red laser due to the narrow emission peak. Furthermore, the red emission peaks ranging from 660 to 730 nm are excited from Cr^{3+} ions in zinc aluminate crystals. The emission peaks at about 687 and 689 nm assigned to R_2 and R_1 lines for the ${}^2\text{E}\rightarrow{}^4\text{A}_2$ transition of Cr^{3+} ions in ideal spinel structure. Due to the antisite defects in spinel lattices, the different crystal fields should result in the other emission peaks with lower energy [7, 21]. The synthesis temperature and the Zn/Al molar ratio reveal the percent of inversion defects in spinel lattices [22, 23], which change the profiles

of emission spectra. With the impurities concentration increasing, the emission intensity can be enhanced, while the emission should be quenched due to the exchange-coupling interaction of Cr–Cr pairs when the dopant concentration is too high [24]. The early studies about the influence of dopant concentration on the PL property supported the single change in the intensity [25, 26].

For the crystals with spinel structure, the increasing dopant concentration should cause more disorder such as inversion defects related to Zn, Al and impurities. The correlational studies are too lacking. Aiming at this, the effects of Cr^{3+} dopant concentration on the structural and PL properties of ZnAl_2O_4 crystals are investigated in this whole paper. The concentration of Cr^{3+} ions reveals obvious influence on the antisite defects related to octahedral Zn, and a new emission peak at about 740 nm is present for zinc aluminate crystal doped with higher concentration of Cr^{3+} ions.

2 Experimental details

The precursor materials were $\text{Zn}(\text{NO}_3)_2\cdot 6\text{H}_2\text{O}$, $\text{Al}(\text{NO}_3)_3\cdot 9\text{H}_2\text{O}$, $\text{CrCl}_3\cdot 6\text{H}_2\text{O}$ and ethylene glycol (EG) were purchased from Shanghai Aladdin Bio-Chem Technology Co., LTD. All the chemicals were analytical reagent (AR) and were used as starting materials without further purification.

The gels with the theoretical composition of $\text{ZnAl}_2\text{O}_4:\text{Cr}^{3+}$ were prepared by using the sol–gel process. Zinc nitrate, aluminum nitrate, chromic chloride were taken in the molar ratio 1: (2– x): x where $x = 0.002, 0.006, 0.01, 0.014, 0.018, 0.022,$ and 0.026 for 0.1, 0.3, 0.5, 0.7, 0.9, 1.1, and 1.3 mol% Cr^{3+} doped compounds, respectively. The stoichiometric quantities of $\text{Al}(\text{NO}_3)_3\cdot 9\text{H}_2\text{O}$ and $\text{Zn}(\text{NO}_3)_2\cdot 6\text{H}_2\text{O}$ were dissolved in 10 ml deionized water respectively, and were stirred for 10 min. Then the Zn (NO_3)₂ solution was dropwise added into $\text{Al}(\text{NO}_3)_3$ solution with vigorous stirring for 20 min, and 20 ml ethylene glycol was added as stabilizer. The obtained transparent solution was divided into seven parts, and a certain amount of CrCl_3 solutions were added into above mixtures and were kept vigorous stirring for 30 min. Then the transparent sols were kept at 250 °C in the oven for about 4 h until became puffed gelation. At last, the puffed products were calcined to obtain $\text{ZnAl}_2\text{O}_4:\text{Cr}^{3+}$ nanophosphors at 1000 °C, and the sintering time was 3 h.

The phase and crystalline nature of the obtained products was investigated using both X-ray diffractometer (XRD) with $\text{Cu}-K_\alpha$ radiation ($\lambda = 0.15406$ nm). The x-ray photoelectron spectroscopy (XPS) analysis was carried out with a Thermol scientific Escalab 250Xi using monochromatized Al X-ray source ($h\nu = 1486.6$ eV, 150 W, diameter beam

spot: 500 μm). The morphologies were characterized by using JEM-2000EX type transmission electron microscope (TEM). The PL spectra were measured with Edinburgh Instruments FLS920 type Spectro-fluorophotometer, in which the excitation wavelength was chosen as 421 and 527 nm. Four hundred and fifty Watts Xe-lamp was used as the exciting light source. Electron paramagnetic resonance (EPR) measurements were carried out using ER-200D-SRC EPR spectrometer operating at the 9.78 GHz X-band frequency.

3 Results and discussion

3.1 X-ray diffraction

Figure 1a shows that the XRD patterns of ZnAl_2O_4 crystals doped with various concentrations of Cr^{3+} ions ranging from 0.1 to 1.3%. With the Cr^{3+} concentration increasing, no extra diffraction peaks related to the Al_2O_3 and ZnO impurities are detected in the patterns, confirming the single phase of the synthesized powder samples with spinel structure (JCPDS, No. 82-1043). The intensity of each diffraction peak has no obvious change for all samples. It is clearly observed that the (311) diffraction peak reveals a clear shift toward lower diffraction angle as shown in Fig. 1b, indicating that the lattice parameters become slightly larger with the Cr^{3+} concentration increasing. According to the previous reports, Cr^{3+} ions likely substitute Al^{3+} ions at the octahedral sites. Comparing the radius of Cr^{3+} (0.63 Å), Zn^{2+} (0.74 Å), and Al^{3+} (0.53 Å), the lattice parameters should increase and the XRD peaks should shift toward the lower angle when the Cr^{3+} ions enter the zinc aluminate lattices. The results suggest that the

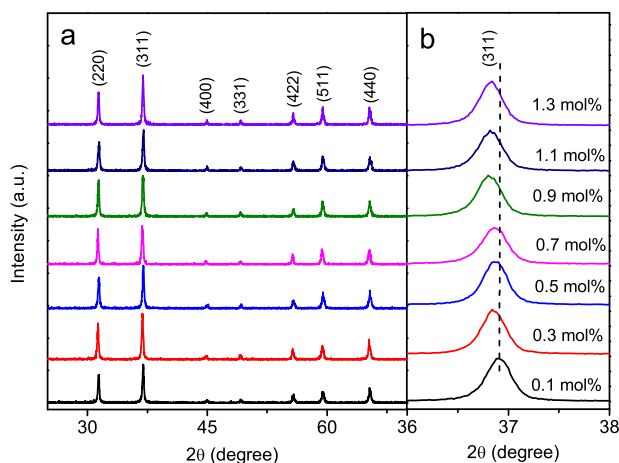


Fig. 1 XRD patterns of ZnAl_2O_4 crystals doped with various concentrations of Cr^{3+} ions. **a** Full XRD patterns and **b** magnified view of (311) diffraction peaks

Cr^{3+} ions are successfully incorporated into the ZnAl_2O_4 lattices.

The crystallinity can be characterized by mean grain size related to the full width at half maximum (FWHM). The mean grain sizes can be calculated according to the Scherrer's equation [23]:

$$D = \frac{0.9\lambda}{\beta \cos\theta}$$

Where D is the mean grain size of the powders, β is the FWHM of diffraction peak, λ is the wavelength of x-ray, and θ is the Bragg's angle. The calculated grain sizes (using (311) diffraction peak) depending on the Cr^{3+} ions concentration are shown in Fig. 2. The grain size reveals a sharp increase from about 27 nm to about 34 nm with the Cr^{3+} ions concentration increasing up to 0.7 mol%, and with a further increase, the Cr^{3+} ions concentration has no obvious influence on the mean grain size which value is keeping at about 34 nm.

3.2 Morphology analysis

Figure 3 shows the SEM images of $\text{ZnAl}_2\text{O}_4:\text{Cr}^{3+}$ crystals (0.1, 0.7, 1.1, and 1.3%, respectively). The increasing concentration of Cr^{3+} dopant has no obvious influence on the morphologies of ZnAl_2O_4 crystals. All samples exhibit a roughly similar particle size of about 100 nm, which is much larger than the calculated mean grain sizes. It might be that these particles should be composed with grain clusters.

In order to investigate the morphology details of $\text{ZnAl}_2\text{O}_4:\text{Cr}^{3+}$ crystals, TEM and high resolution TEM (HRTEM) measurements have been carried out and the images of ZnAl_2O_4 crystals doped with 0.1 mol% and 1.3 mol% Cr^{3+} are shown in Fig. 4, respectively. The results

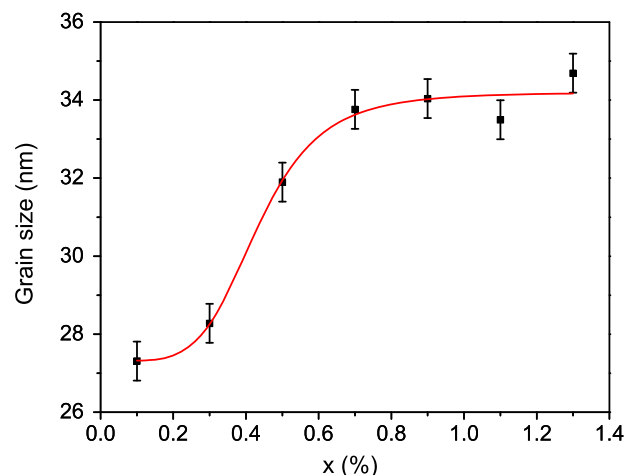


Fig. 2 The calculated mean grain sizes of ZnAl_2O_4 crystals doped with various concentrations of Cr^{3+} ions

Fig. 3 SEM images of $\text{ZnAl}_2\text{O}_4:\text{Cr}^{3+}$ crystals doped with various concentrations of Cr^{3+} ions. **a** 0.1 mol%; **b** 0.7 mol%; **c** 1.1 mol% and **d** 1.3 mol%

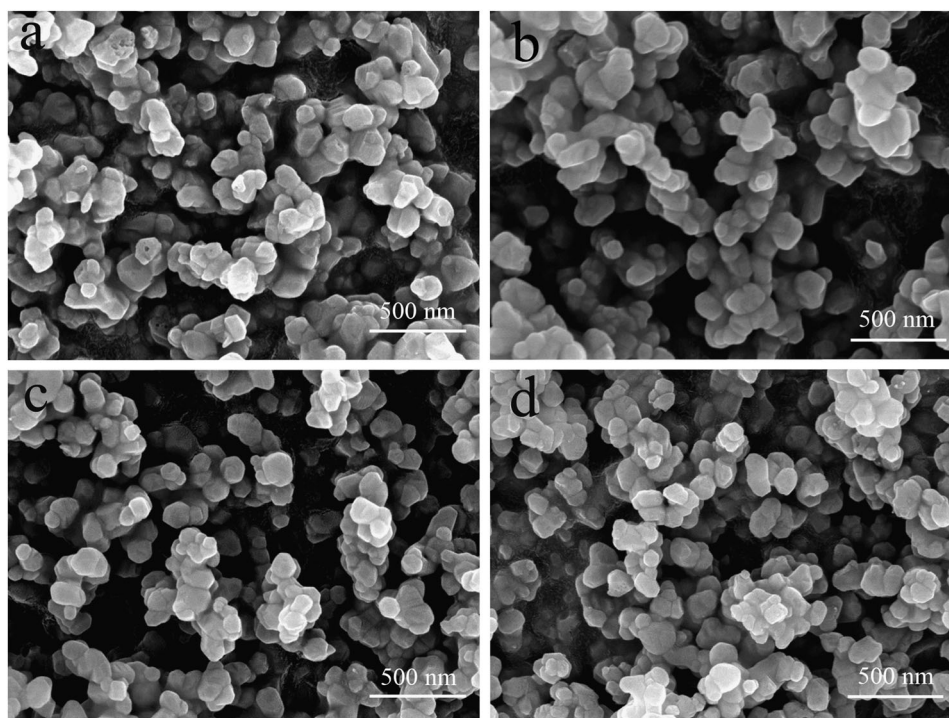
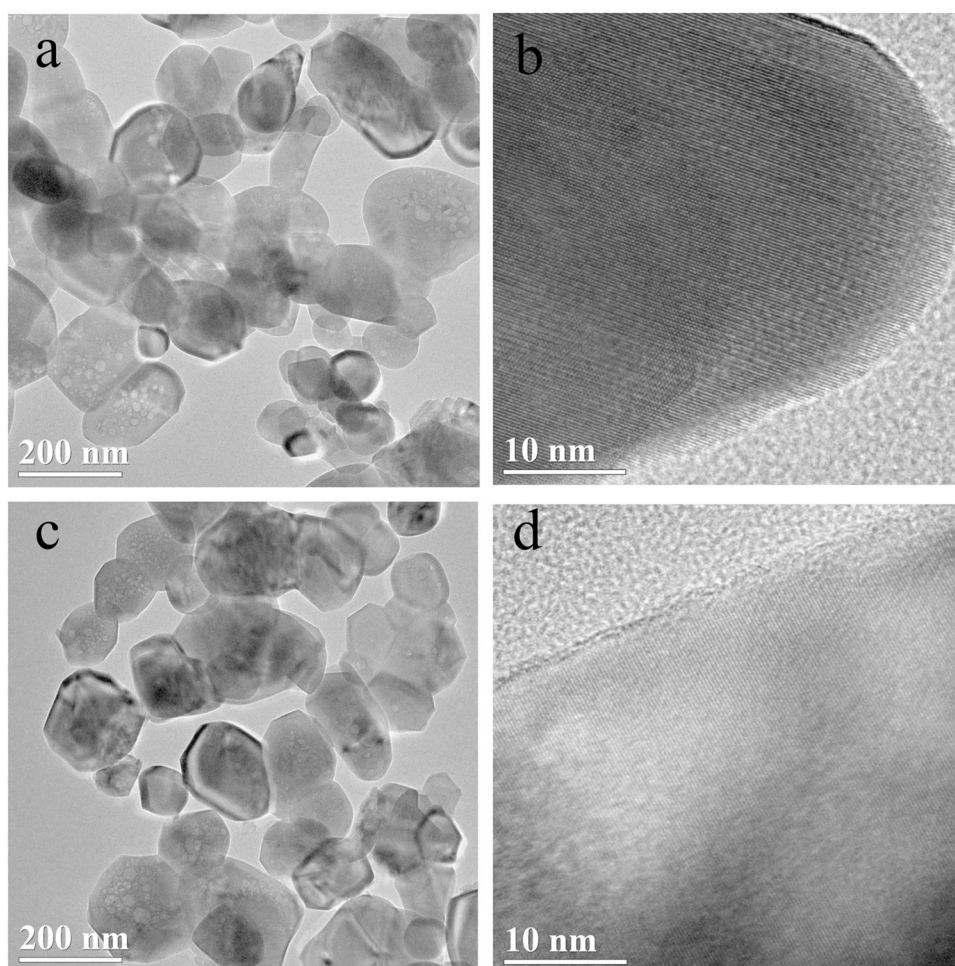


Fig. 4 HRTEM images of ZnAl_2O_4 crystals doped with **a–b** 0.1 mol% and **c–d** 1.3 mol% Cr^{3+} ions



show that the crystal sizes are non-uniform and there are some tiny crystals presenting on the surface of the larger crystals. Compared with the results of SEM, larger grains reveal similar size between these powders. While for the powder with 0.1 mol% Cr³⁺ ions, the amount of grains with smaller size is less than that of the powders with 1.3 mol% Cr³⁺ ions, which should result in the different mean grain size comparing with the results of XRD. The results from the HRTEM (Fig. 4b, d) show that the ZnAl₂O₄:Cr³⁺ (1.3 mol%) crystals have disordered surface lattices, indicating that the surface defects increase with the concentration of Cr³⁺ ions increasing.

3.3 X-ray photoelectron spectroscopy

The elemental compositions of the powders are further determined by using XPS, and the results are shown in Fig. 5. The XPS survey spectrum confirms the presence of Al, O, Zn, Cr, and C in the crystals. Figure 6 shows the high-resolution XPS spectra and the fitted curves for the O 1s peak from ZnAl₂O₄:Cr³⁺ crystal with Cr³⁺ concentration ranging from 0.1 to 1.3 mol%. The experimental dots are fitted well with two Gaussian peaks at about 530.5 and 532.2 eV. According to the results from Tshabalala et al. [14] and Cabello et al. [27], because of the environmental moisture, the higher-energy peak corresponds to O–H bonds from absorbed water molecules, and the lower-energy peak is attributed to metal-oxygen bonds assigned to the spinel lattices.

Figure 7 shows the high-resolution XPS spectra of Al 2p region for ZnAl₂O₄:Cr³⁺ crystals. For all of the samples, the experimental data can be fitted well with single Gaussian peak whose center is about 73.5 eV. Tshabalala et al. [14] observed the Al_{2p} peaks with the binding energies of 74.2 and 75.6 eV assigned to the Al³⁺ ions occupying the tetrahedral ([AlO₄] group, Al_{Zn}) and octahedral sites ([AlO₆] group), respectively, in ZnAl₂O₄:Ce³⁺, Tb³⁺ crystals.

Cabello et al. [27] detected the Al 2p peaks as a broad and asymmetric band at about 74.1 eV in zinc aluminate crystals. Iacche et al. [28] found that the binding energy shifted from 74.0 to 74.7 eV in ZnO/ZnAl₂O₄ crystals with annealing temperature increasing from 650 to 700 °C. Considering different crystal fields caused by different dopants and various defects in spinel lattices, the peak at 73.5 eV should be assigned to Al³⁺ ions occupying in octahedral sites in ZnAl₂O₄:Cr³⁺ crystals. The shift of Al 2p peak should be resulted from the Zn-antisite defects.

Figure 8 shows the XPS spectra of the Zn 2p region for ZnAl₂O₄ crystals with various Cr³⁺ dopant concentrations. The Zn 2p core level spectrum shows a doublet ranging from 1020 to 1027 eV and from 1043 to 1050 eV, which can be identified as the Zn 2p_{3/2} and Zn 2p_{1/2} lines, respectively [29]. Both peaks can be fitted well by using

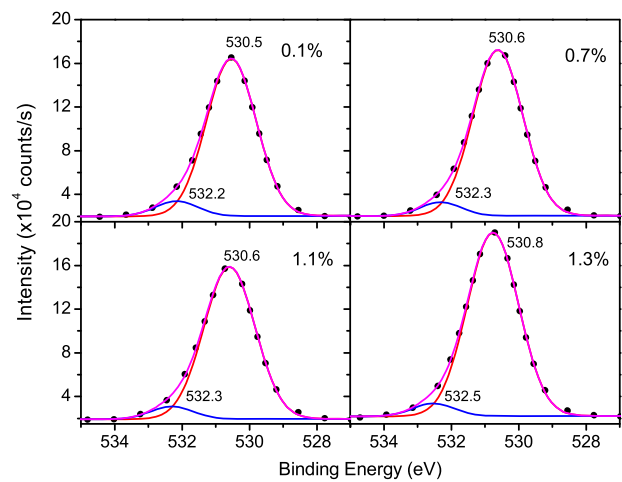


Fig. 6 The experimental dots and fitted curves of high-resolution XPS spectra of O 1s in ZnAl₂O₄: Cr³⁺ crystals

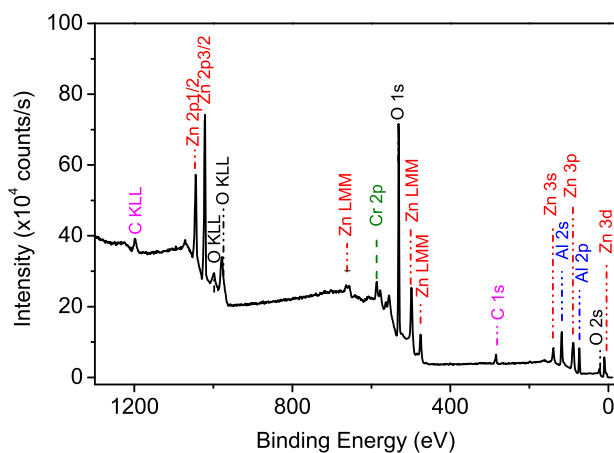


Fig. 5 XPS survey spectrum of ZnAl₂O₄:Cr³⁺ (0.1 mol%) crystals

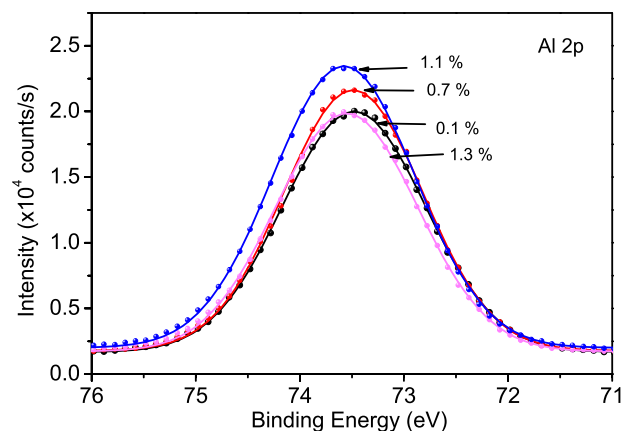


Fig. 7 The experimental dots and fitted curves of high-resolution XPS spectra of Al 2p in ZnAl₂O₄: Cr³⁺ crystals

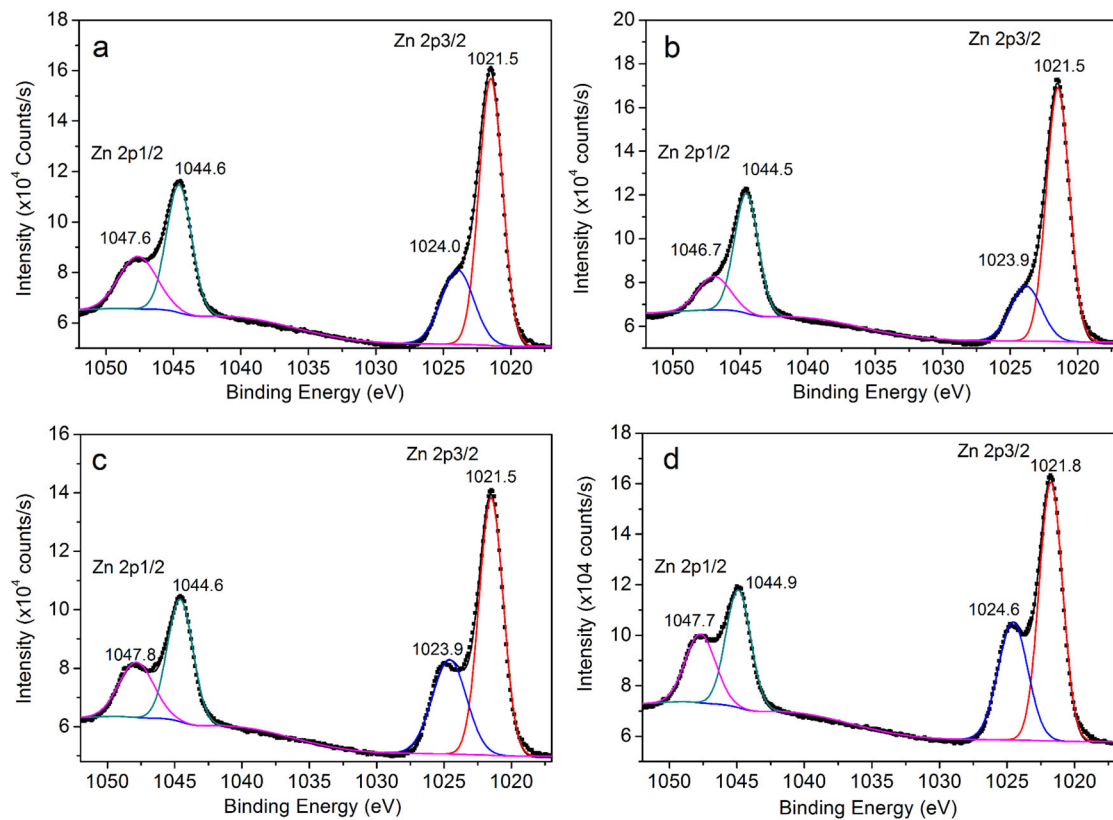


Fig. 8 The experimental dots and fitted curves of high-resolution XPS spectra of Zn 2p_{3/2} and Zn 2p_{1/2} in ZnAl₂O₄ crystals with various Cr³⁺ dopants. **a** 0.1 mol%; **b** 0.7 mol%; **c** 1.1 mol%; **d** 1.3 mol%

two Gaussian peaks as shown in Fig. 8. The fitted center energies are 1021.5 and 1023.9 eV for Zn 2p_{3/2} line, and 1044.6 and 1047.8 eV for Zn 2p_{1/2} line, respectively. The peaks at 1021.5 and 1044.6 eV are assigned to tetrahedral Zn²⁺ ions ([ZnO₄] group), and these peaks at 1024.0 and 1047.6 eV are assigned to octahedral Zn²⁺ ions ([ZnO₆] group, Zn_{Al}) [29]. The concentrations of unperturbed Zn ions in spinel lattices are 72%, 77%, 66% and 63% for the powders with 0.1, 0.7, 1.1, and 1.3 mol% Cr³⁺ dopants, respectively. The values are much larger than the standard stoichiometry of Zn ions in perfect zinc aluminate lattices as well as the molar concentration of Zn in precursors. It indicates that there are octahedral Zn defects existing in the surface lattices of ZnAl₂O₄:Cr³⁺ crystals, and with the concentration of Cr³⁺ dopant increasing, these antisite defects increase.

Sreeja et al. [9] investigated the size dependence of coordination behavior and cation distribution in MgAl₂O₄ nanoparticles from ²⁷Al solid state NMR. The results showed that the defects related to Al³⁺ ions in the tetrahedral sites existed on the surface of MgAl₂O₄ nanoparticles, especially when grain size was below 18 nm. With the grain size increasing, the percentage of Al³⁺ ions in the tetrahedral sites decreased, meanwhile, the indirect

evidences suggested that the additional octahedral sites related the [AlO₆] octahedra surrounding [MgO₆] octahedra (Mg_{Al}). The theoretical results from Dixit et al. [8] showed that the antisite defects related to Al_{Zn} and Zn_{Al} had the lowest formation energy of all native defects in ZnAl₂O₄ lattices, and the formation energy of Al_{Zn} was lower than that of Zn_{Al} due to the smaller radius of Al³⁺ ions.

The experimental dots and fitted curves of high-resolution XPS spectra of Cr 2p are shown in Fig. 9. Two binding energy centers are at about 586.3 and 577.0 eV, which are assigned to Cr³⁺ ions [30]. With the Cr³⁺ concentration increasing from 0.1 to 1.3 mol%, the peak centers shift from 586.3 to 586.5 eV and from 577.0 to 577.1 eV, respectively, indicating that the surrounding of Cr³⁺ ions in spinel structure should be changed. These results are corresponding to the XPS results of Zn 2p. The results of XPS suggest that the Cr³⁺ concentration results in the increase of inversion defects related to Zn_{Al} in surface lattices of zinc aluminate crystals.

3.4 Electronic paramagnetic resonance

In order to investigate the sites of Cr³⁺ ions in spinel lattices, the EPR measurements with external magnetic field

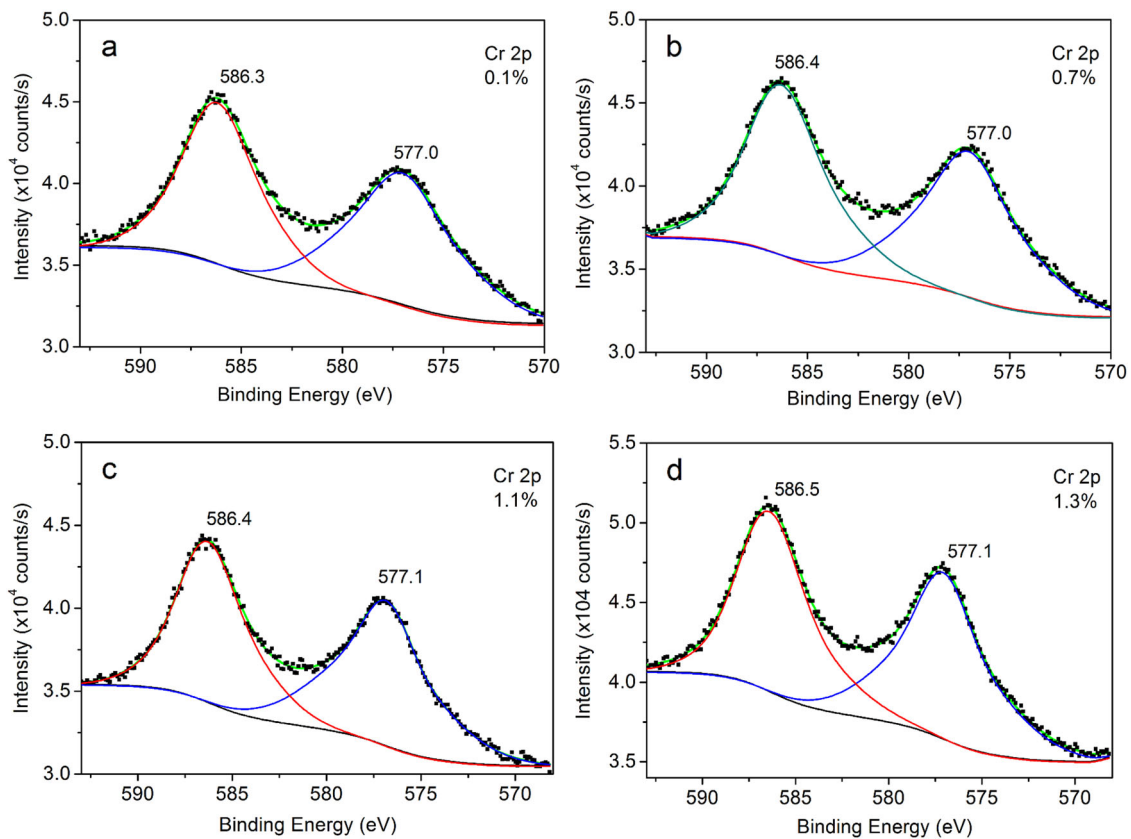


Fig. 9 The experimental dots and fitted curves of high-resolution XPS spectra of Cr 2p in $\text{ZnAl}_2\text{O}_4:\text{Cr}^{3+}$ crystals. **a** 0.1 mol%; **b** 0.7 mol%; **c** 1.1 mol%; **d** 1.3 mol%

ranging from 50 to 550 mT were carried out. The results of EPR for the ZnAl_2O_4 crystals with different Cr^{3+} dopant concentrations are shown in Fig. 10. A strong resonance peak at about 174 mT is detected for each sample, which corresponds to the effective gyromagnetic ratio at $g = 3.84$ for the Cr^{3+} ions in spinel lattices [31, 32]. The increasing intensity of the signal at about $g = 3.84$ suggests that the amount of emission centers in spinel lattices increases. It is noted that, with Cr^{3+} dopant concentration increasing, the resonance field reveals an obvious shift toward higher magnetic field from 174.28 to 175.14 mT. The surroundings of Cr^{3+} ions sites should be changed, and the peak-to-peak value (B_{p-p}) of resonance signal becomes wider from 4.5 to 6.9 mT. This could be more defects are present in zinc aluminate lattices. Both of these results are agree with the results of XPS. Additionally, a signal at $g = 1.97$ assigned to coupling Cr–Cr pairs in spinel lattices is present, and the signal intensity is enhanced with increasing Cr^{3+} ions concentrations [31, 32], indicating that the exchange-coupling interaction between Cr^{3+} ions is enhanced due to more Cr^{3+} dopants in lattices. For the zinc aluminate crystals with the same Cr^{3+} dopant concentration, the stronger interaction between Cr^{3+} ions should result in the photoluminescence quenching. It is noteworthy that both

resonance signals for the samples with Cr^{3+} dopant concentrations ranging from 0.7 to 0.9 mol% have the generally same intensity as shown in the inset of Fig. 10a. When the Cr^{3+} ions concentration is above 0.1 mol%, a series of satellite resonance peaks are detected around the main resonance peak at $g = 3.84$. Unlike the signals at $g = 3.84$ and $g = 1.97$, the intensity of these satellite peaks reveals a continuous enhancement with the Cr^{3+} ions concentration increasing from 0.1 to 1.3%. According to the results from Gourier et al., these satellite peaks should come from the defects related to $\text{Zn}_{\text{Al}}-\text{Cr}^{3+}$. It indicates that the Cr–Cr coupling pairs and the inversion defects are coexist in $\text{ZnAl}_2\text{O}_4:\text{Cr}^{3+}$ crystals due to the octahedral Zn.

3.5 Photoluminescence analysis

The typical PL excitation (PLE) spectra of $\text{ZnAl}_2\text{O}_4:\text{Cr}^{3+}$ crystals are shown in Fig. 11a. With monitoring the emission at 687 nm, two main excitation peaks are detected, which the center positions are 400 and 534 nm, respectively. The broad band centered at 534 nm is assigned at ${}^4\text{A}_{2g}(\text{F}) \rightarrow {}^4\text{T}_{2g}(\text{F})$, and the other broad band at 400 nm is assigned at ${}^4\text{A}_{2g}(\text{F}) \rightarrow {}^4\text{T}_{1g}(\text{F})$ transition of Cr^{3+} ions in

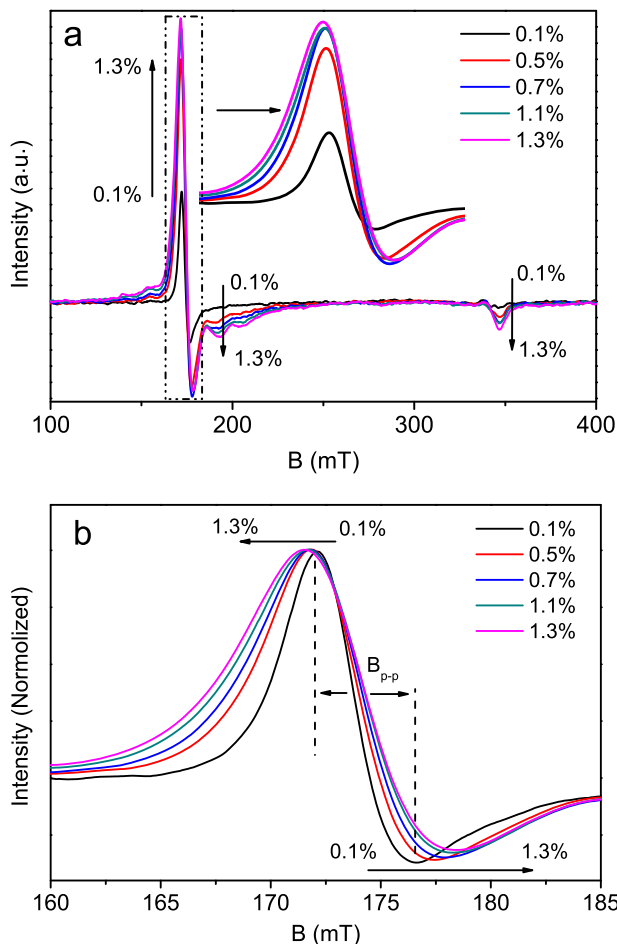


Fig. 10 **a** EPR spectra of ZnAl_2O_4 crystals doped with various Cr^{3+} concentrations and **b** the profiles of normalized signals at 174 mT. The inset in **a** is the modified profiles of resonance signal at about 174 mT

spinel lattices [10, 31]. Therefore, we assume that the Cr^{3+} ions enter the lattices of zinc aluminate crystals.

Figure 11b exhibits the PL spectra of $\text{ZnAl}_2\text{O}_4:\text{Cr}^{3+}$ (0.1%) crystals with different excitation wavelengths. A series of emission peaks is observed from 660 to 730 nm, and the emission spectra show the same profile and wavelength but different intensity. The emissions at 687 and 689 nm are two zero phonon (ZP) lines known as R_2 and R_1 for the ${}^2E \rightarrow {}^4A_2$ transition of Cr^{3+} occupying the octahedral Al sites [21, 33]. The phonon side bands (PSB) of the R lines were observed in emission spectra at the region from 667 to 680 nm for the Anti-Stokes PSB and at the region from 709 to 723 nm for the Stokes PSB [33]. Additional emission peaks at 695 and 699 nm are detected as shown in Fig. 11b. The defects related to Al occupying Zn sites and Zn occupying Al sites also cause the different surroundings of Cr^{3+} ions, which induce the new emissions appearance in the longer wavelength region attributed to N lines. Bessière et al. [21] have showed lower energy at a line marked as N_2 for Cr^{3+} lies at 147 cm^{-1} than R_1 . Our results are agreed

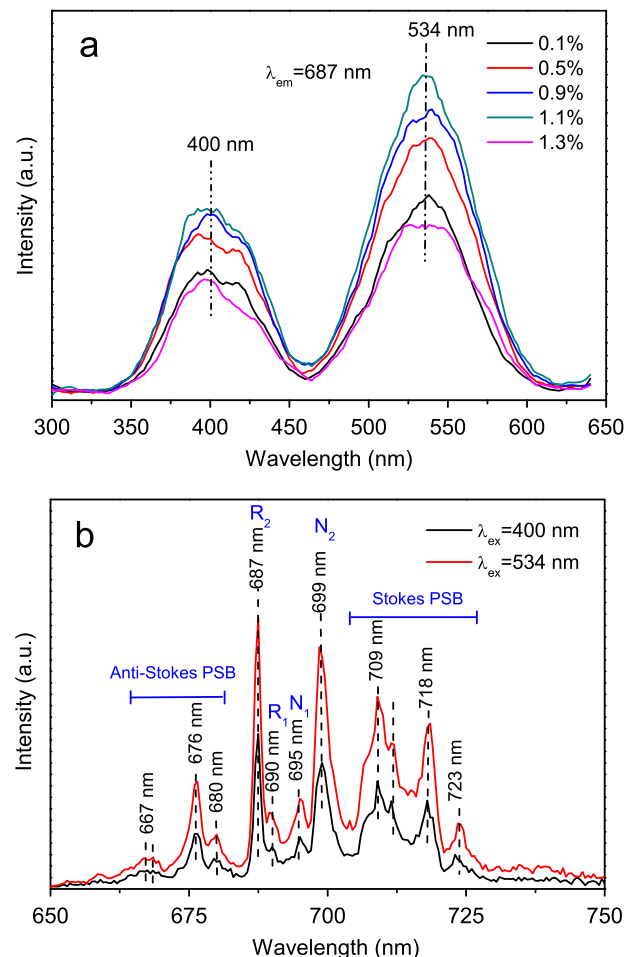


Fig. 11 **a** PL excitation spectra of $\text{ZnAl}_2\text{O}_4:\text{Cr}^{3+}$ crystals with various Cr^{3+} concentrations; **b** PL spectra of $\text{ZnAl}_2\text{O}_4:\text{Cr}^{3+}$ (0.1 mol%) crystals with different excitation wavelengths

well with the results from Bessière et al. [21]. We therefore attribute these two lines to the N_2 lines of Cr^{3+} . According to the results of XPS and EPR, the defects are assigned to the inversion defects related to Zn occupying Al sites.

In order to investigate the influence of Cr^{3+} concentration on the PL property of zinc aluminate crystals, the PL spectra of ZnAl_2O_4 crystals doped with various Cr^{3+} concentrations are detected and the results are shown in Fig. 12. With the Cr^{3+} dopant concentration increasing from 0.1% to 0.7%, the intensity of PL spectra increase, and sharply decreases when the concentration reach to 1.3 mol%. We note that the PL spectra stay constant in the intensity when the concentration of Cr^{3+} ions increases from 0.7 to 1.1 mol%. However, the intensity of the PL spectra ranging from 730 to 750 nm show a clear increase and a new emission peak at about 740 nm is present and its intensity continuously increases with the Cr^{3+} ions concentration increasing from 0.1 to 1.3 mol%. The emissions are quenched when the concentration of Cr^{3+} ions is at 1.3 mol% for all samples. The increasing intensity of R lines and N lines

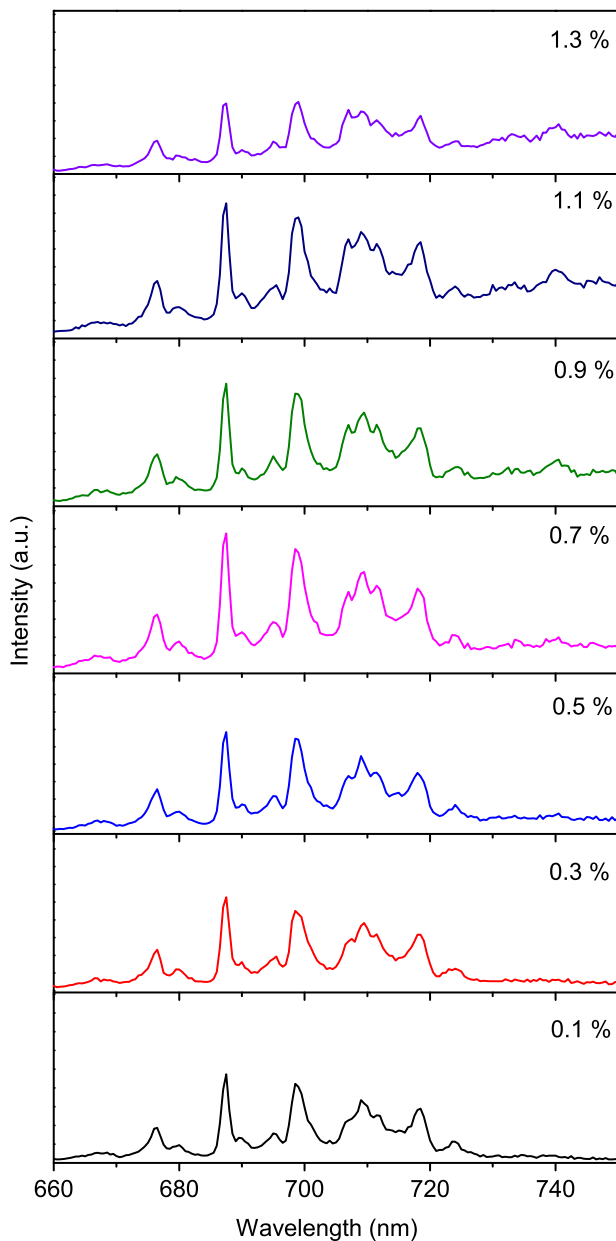


Fig. 12 PL spectra of ZnAl₂O₄ crystals with various Cr³⁺ concentrations

should result from the increase of emission centers (Cr³⁺ ions) in spinel lattices.

The relative intensity of all PL spectra comparing to the R₂ line is shown in Fig. 13. The relative intensity of N₂ lines and Stokes PSB lines comparing to the intensity of R₂ line increases with Cr³⁺ concentration increasing as shown in Fig. 13. The increasing intensity of N₂ lines indicates that the antisite defects increase in spinel lattices. According to the results of XPS, the antisite defects should be related to octahedral Zn. In order to investigate the origin of the emission peak at 740 nm, the PLE spectra of ZnAl₂O₄: 1.3 mol% Cr³⁺ crystals are detected with monitoring the

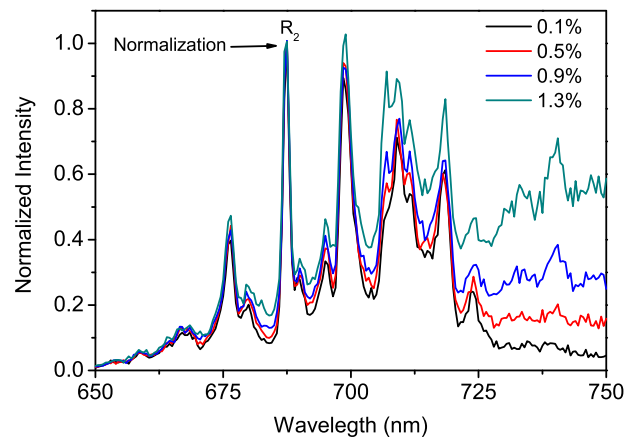


Fig. 13 Normalized PL spectra of ZnAl₂O₄ crystals doped with various Cr³⁺ concentrations

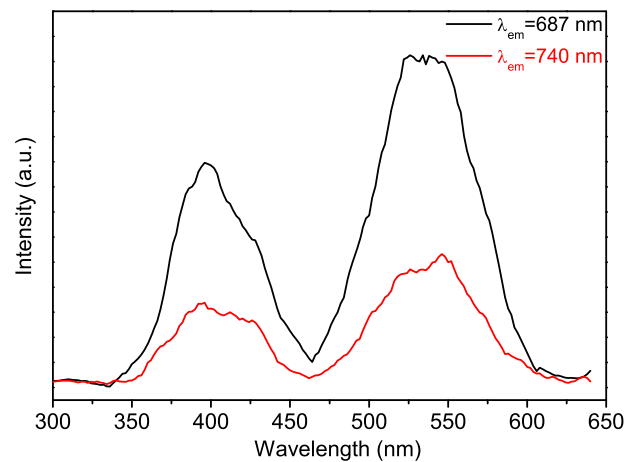


Fig. 14 PLE spectra of ZnAl₂O₄:Cr³⁺ (1.3 mol%) crystals with emission wavelengths of 687 nm and 740 nm, respectively

emissions at 687 and 740 nm, and the results are shown in Fig. 14. Both spectra reveal similar profiles and center positions but different intensity, which the emission at 740 nm is assigned to the Cr³⁺ ions in spinel lattices. According to the results of EPR, the emission at 740 nm should result from the interaction between Cr–Cr pairs in the spinel structure.

4 Conclusions

In summary, ZnAl₂O₄ crystals doped with various concentrations of Cr³⁺ ions were successfully fabricated by using sol–gel method. The dopant of Cr³⁺ ions resulted in more uniform grains, which induced the larger mean grain size with the doping concentration increasing. While the increasing concentration of Cr³⁺ ions caused more antisite defects related to octahedral Zn in surface lattices of zinc aluminate. The PL spectra were enhanced with the

concentration of Cr^{3+} ions due to the amount of emission centers increasing. The Cr–Cr pairs were detected with the Cr^{3+} ions concentration increasing, which caused that the PL spectra revealed similar intensity due to their quenching effect on the PL properties, and with the concentration of Cr^{3+} ions increasing further, the PL spectra were quenched due to the larger number of Cr–Cr pairs in spinel structure. The new emission peak at 740 nm was observed and should result from the interaction of Cr–Cr pairs.

Acknowledgements This work was supported by Initial Foundation for Doctor Programme of Liaocheng University (No. 318051410), the Project of Science and Technology Plan for University of Shandong Province (No. J16LJ05), the National Natural Science Foundation of China (No. 61574071, No. 11604132, No. 11604133), and Industrial Alliance Fund of Shandong Provincial Key Laboratory (Grant No. SDKL2016038), and the Special Construction Project Fund for Shandong Province Taishan Scholars.

Compliance with ethical standards

Conflict of interest The authors declare that they have no competing interests.

References

- Pathak N, Gupta SK, Sanyal K, Kumar M, Kadam RM, Natarajan V (2014) Photoluminescence and EPR studies on Fe^{3+} doped ZnAl_2O_4 : an evidence for local site swapping of Fe^{3+} and formation of inverse and normal phase. *Dalton Trans* 43:9313–9323
- Motloung SV, Dejene FB, Swart HC, Ntwaeaborwa OM (2015) Effects of Cr^{3+} mol% on the structure and optical properties of the $\text{ZnAl}_2\text{O}_4:\text{Cr}^{3+}$ nanocrystals synthesized using sol-gel process. *Ceram Int* 41:6776–6783
- Cheng BC, Qu SC, Zhou HY, Wang ZG (2006) Porous ZnAl_2O_4 spinel nanorods doped with Eu^{3+} : synthesis and photoluminescence. *Nanotechnology* 17:2982–2987
- Battistona S, Rigoa C, Severoa EC, Mazuttia MA, Kuhna RC, Gündelb A, Foletto EL (2014) Synthesis of Zinc Aluminate (ZnAl_2O_4) spinel and its application as photocatalyst. *Mater Res* 17:734–738
- Singh RK, Yadav A, Narayan A, Chandra M, Verma RK, Thermal (2012) XRD, and magnetization studies on ZnAl_2O_4 and NiAl_2O_4 spinels, synthesized by citrate precursor method and annealed at 450 and 650 °C. *J Therm Anal Calorim* 107:205–210
- Joo OS, Jung KD (2003) Stability of ZnAl_2O_4 catalyst for reverse-water-gas-shift reaction (RWGSR). *Bull Korean Chem Soc* 24:86–90
- Gourier D, Bessière A, Sharma SK, Binet L, Viana B, Basavaraju N, Priolkar KR (2014) Origin of the visible light induced persistent luminescence of Cr^{3+} -doped zinc gallate. *J Phys Chem Solids* 75:826–837
- Dixit H, Tandon N, Cottenier S, Saniz R, Lamoen D, Partoens B (2013) First-principles study of possible shallow donors in ZnAl_2O_4 spinel. *Phys Rev B* 87:174101
- Sreeja V, Smitha TS, Nand D, Ajithkumar TG, Joy PA (2008) Size dependent coordination behavior and cation distribution in MgAl_2O_4 nanoparticles from ^{27}Al solid state NMR studies. *J Phys Chem C* 112:14737–14744
- Brik MG, Papan J, Jovanovic DJ, Dramicanin MD (2016) Luminescence of Cr^{3+} ions in ZnAl_2O_4 and MgAl_2O_4 spinels: correlation between experimental spectroscopic studies and crystal field calculations. *J Lumin* 177:145–151
- Rojas-Hernandez RE, Rubio-Marcos F, Rezende MV, Rodriguez MÁ, Serrano A, Muñoz-Noval Á, Fernandez JF (2016) The impact of the synthesis conditions on $\text{SrAl}_2\text{O}_4:\text{Eu}$, Dy formation for a persistent afterglow. *Mater Des* 108:354–363
- Fernández-Osorio A, Rivera CE, Vázquez-Olmos A, Chávez J (2015) Luminescence ceramic nano-pigments based on terbium-doped zinc aluminate: synthesis, properties and performance. *Dyes Pigments* 119:22–29
- Prusty RK, Kuruva P, Ramamurty U, Thomas T (2013) Correlations between mechanical and photoluminescence properties in Eu doped sodium bismuth titanate. *Solid State Commun* 173:38–41
- Tshabalala KG, Cho SH, Park JK, Pitale SS, Nagpure IM, Kroon RE, Swart HC, Ntwaeaborwa OM (2011) Luminescent properties and X-ray photoelectron spectroscopy study of $\text{ZnAl}_2\text{O}_4:\text{Ce}^{3+}, \text{Tb}^{3+}$ phosphor. *J Alloys Comp* 509:10115–10120
- Zhang D, Wang CZ, Liu YL, Shi Q, Wang WJ, Zhai Y (2012) Green and red photoluminescence from $\text{ZnAl}_2\text{O}_4:\text{Mn}$ phosphors prepared by sol-gel method. *J Lumin* 132:1529–1531
- Yu YL, Li XY (2016) Controllable synthesis tunable luminescence of glass ceramic containing $\text{Mn}^{2+}:\text{ZnAl}_2\text{O}_4$ and $\text{Pr}^{3+}:\text{YF}_3$ nano-crystals. *Mater Res Bull* 73:96–101
- Zhang D, Yin YL, Liu YL, Chao WB, Zhai Y (2013) The photoluminescence and magnetic properties of $\text{ZnAl}_2\text{O}_4:\text{Mn}$ nanocrystals. *J Phys Chem Solids* 74:1131–1135
- Anand GT, Kennedy LJ, Vijaya JJ (2013) Microwave combustion synthesis, structural, optical and magnetic properties of $\text{Zn}_{1-x}\text{Co}_x\text{Al}_2\text{O}_4$ ($0 \leq x \leq 0.5$) spinel nanostructures. *J Alloys Comp* 581:558–566
- Tsai MT, Chang YS, Chou YH, Tsai KM (2014) Photoluminescence of titanium-doped zinc spinel blue-emitting nanophosphors. *J Solid State Chem* 214:86–90
- Dereñ PJ, Stefańska D, Ptak M, maczka M, Walerczyk W, Banach G (2014) Origin of violet-blue emission in Ti-doped Gahnite. *J Am Ceram Soc* 97:1883–1889
- Basavaraju N, Priolkar KR, Gourier D, Sharma SK, Bessière A, Viana B (2015) Importance of inversion disorder in visible light induced persistent luminescence in Cr^{3+} doped AB_2O_4 ($A=\text{Zn}$ or Mg and $B=\text{Ga}$ or Al). *Phys Chem Chem Phys* 17:1790–1799
- Zhang Q, Ma XX, Zhang Q, Xie YR, Shi Q, Wang QR, Wang WJ (2016) Influence of Zn/Al molar ratio on the structural and photoluminescence performances of $\text{Zn}_x\text{Al}_2\text{O}_4:\text{Cr}^{3+}$ phosphors. *J Alloy Comp* 688:581–587
- Zhang D, Qiu YH, Xie YR, Zhou XC, Wang QR, Shi Q, Li SH, Wang WJ (2017) The improvement of structure and photoluminescence properties of $\text{ZnAl}_2\text{O}_4:\text{Cr}^{3+}$ ceramics synthesized by using solvothermal method. *Mater Des* 115:37–45
- Marquês da Silva MAF, Silva Pedro S, Sosman LP (2010) Cr^{3+} impurity concentration and excitation dependence of magnesium gallate spinel photoluminescent data. *J Alloy Comp* 492:282–285
- Rojas-Hernandez RE, Rubio-Marcos F, Rezende MV, Rodriguez MÁ, Serrano A, Muñoz-Noval Á, Fernandez JF (2016) The impact of the synthesis conditions on $\text{SrAl}_2\text{O}_4:\text{Eu}$, Dy formation for a persistent afterglow. *Mater Des* 108:354–363
- Marquês da Silva MAF, Silva Pedro S, Sosman LP (2010) Cr^{3+} impurity concentration and excitation dependence of magnesium gallate spinel photoluminescent data. *J Alloy Comp* 492:282–285
- Cabello G, Lillo L, Caro C, Seguel M, Sandoval C, Buono-Core GE, Chornik B, Flores M (2016) A photochemical proposal for the preparation of ZnAl_2O_4 and MgAl_2O_4 thin films from β -diketonate complex precursors. *Mater Res Bull* 77:212–220

28. Iaiche S, Djelloul A (2015) ZnO/ZnAl₂O₄ nanocomposite films studied by X-ray diffraction, FTIR, and X-ray photoelectron spectroscopy. *J Spect* 2015:836859
29. Duan XL, Yuan DR, Xu FP (2011) Cation distribution in co-doped ZnAl₂O₄ nanoparticles studied by X-ray photoelectron spectroscopy and ²⁷Al solid-state NMR spectroscopy. *Inorg Chem* 50:5460–5467
30. Benito N, Díaz D, Vergara L, Galindo RE, Sánchez O, Palacio C (2011) An XPS and ellipsometry study of Cr-O-Al mixed oxides grown by reactive magnetron sputtering. *Surf Coat Technol* 206:1484–1489
31. Singh V, Chakradhar RPS, Rao JL, Kwak HY (2011) EPR and photoluminescence properties of combustion-synthesized ZnAl₂O₄:Cr³⁺ phosphors. *J Mater Sci* 46:2331–2337
32. Singh V, Sivaramaiah G, Rao JL, Kim SH (2014) EPR and optical investigations of LaMgAl₁₁O₁₉:Cr³⁺ phosphor. *Mater Res Bull* 60:397–400
33. Bessière A, Jacquart S, Priolkar K, Lecointre A, Viana B, Gourier D (2011) ZnGa₂O₄:Cr³⁺: a new red long-lasting phosphor with high brightness. *Opt Exp* 19:10131–10137